Published in final edited form as:

Mol Imaging Biol. 2015 October ; 17(5): 609–614. doi:10.1007/s11307-015-0836-6.

Imaging Chronic Tuberculous Lesions Using Sodium [^{18}F]Fluoride Positron Emission Tomography in Mice

Alvaro A. Ordonez[1,2,3], **Vincent P. DeMarco**[1,2,3], **Mariah H. Klunk**[1,2,3], **Supriya Pokkali**[1,2,3], and **Sanjay K. Jain**[1,2,3]

Sanjay K. Jain: sjain5@jhmi.edu

[1]Center for Infection and Inflammation Imaging Research, Johns Hopkins University, 1550 Orleans Street, CRB-II, Rm 1.09, Baltimore, MD, USA

[2]Center for Tuberculosis Research, Johns Hopkins University, Baltimore, MD, USA

[3]Department of Pediatrics, Johns Hopkins University, Baltimore, MD, USA

Abstract

Purpose—Calcification is a hallmark of chronic tuberculosis (TB) in humans, often noted years to decades (after the initial infection) on chest radiography, but not visualized well with traditional positron emission tomography (PET). We hypothesized that sodium [^{18}F]fluoride (Na[^{18}F]F) PET could be used to detect microcalcifications in a chronically *Mycobacterium tuberculosis*-infected murine model.

Procedures—C3HeB/FeJ mice, which develop necrotic and hypoxic TB lesions, were aerosolinfected with *M. tuberculosis* and imaged with Na[^{18}F]F PET.

Results—Pulmonary TB lesions from chronically infected mice demonstrated significantly higher Na[^{18}F]F uptake compared with acutely infected or uninfected animals ($P<0.01$), while no differences were noted in the blood or bone compartments ($P>0.08$). *Ex vivo* biodistribution studies confirmed the imaging findings, and tissue histology demonstrated microcalcifications in TB lesions from chronically infected mice, which has not been demonstrated previously in a murine model.

Conclusion—Na[^{18}F]F PET can be used for the detection of chronic TB lesions and could prove to be a useful noninvasive biomarker for TB studies.

Keywords

Tuberculosis; Chronic; Na[^{18}F]F; Microcalcification; PET

Correspondence to: Sanjay K. Jain, sjain5@jhmi.edu.

Electronic supplementary material The online version of this article (doi:10.1007/s11307-015-0836-6) contains supplementary material, which is available to authorized users.

Conflict of Interest. None of the authors report any financial or potential conflicts of interest.

Electronic Supplementary Material: Below is the link to the electronic supplementary material.ESM 1(PDF 66 kb) ESM 2(MOV 639 kb) ESM 3(MOV 1118 kb)ESM 4 (MOV 625 kb)

M*ycobacterium tuberculosis* continues to rage globally and was responsible for an estimated 9 million new cases of active tuberculosis (TB) and 1.5 million deaths in 2013 [1]. It is estimated that one third of the world's population has latent TB infection. These individuals are asymptomatic and harbor dormant *M. tuberculosis*, which can reactivate and cause active TB decades after the initial infection.

TB in humans is characterized by a complex spectrum of disease with multiple pathologies including pneumonias, discrete granulomatous lesions with caseous necrosis and cavitation, as well as more quiescent chronic lesions with calcification [2, 3]. Positron emission tomography (PET) can add functional molecular information to traditional anatomic methods and has provided novel insights into TB pathology [4–6]. Since calcification is a hallmark of chronic TB that is difficult to visualize using traditional PET techniques [7], we assessed the ability of sodium [^{18}F]fluoride (Na[^{18}F]F) PET to visualize microcalcifications in chronic TB lesions in the C3HeB/FeJ mouse model, which develops necrotic and hypoxic TB lesions [8, 9].

Materials and Methods

All protocols were approved by the Johns Hopkins Biosafety, Radiation Safety, and Animal Care and Use Committees.

Four- to six-week-old female C3HeB/FeJ (Jackson Laboratory) mice were aerosol-infected with *M. tuberculosis* H37Rv using the Middlebrook Inhalation Exposure System (Glas-Col) with frozen titrated bacterial stocks. Mice were sacrificed to determine the pulmonary bacillary burden as colony-forming units (CFU) 1 day after infection and at each imaging time point (8 weeks postinfection for acute, and 28–36 weeks post-infection for the chronically infected, animals) as described previously [10, 11]. At least three mice were used for each group per time point.

A separate cohort of similarly infected (live) mice were imaged within sealed bio-containment devices using methods described previously [10, 12]. Each mouse was weighed, injected with 8.5 MBq of Na[^{18}F]F (IBA Molecular) *via* the tail vein, and imaged 10 min post-injection using the Mosaic HP (Philips) small-animal PET with a 55-min dynamic acquisition protocol (11 5-min frames). A computed tomography (CT) scan was also performed subsequently using the NanoSPECT/CT (Bioscan) animal imager. Image analyses were performed as described previously [11, 13–15]. Briefly, PET images were reconstructed (3D-RAMLA) and coregistered with CT images using VivoQuant 1.23 (inviCRO). Using the CT images as a reference, spherical regions of interest (ROI 3 mm diameter) were drawn around pulmonary lesions, heart—left ventricle (blood), and thoracic vertebrae (bone) and applied to the PET images with correction for partial volume effect. Standardized uptake values (SUV) were computed using Amide version 1.0.4 (www.amide.sourceforge.net). After imaging, mice were sacrificed to collect tissues for direct gamma counting (biodistribution) and data is presented as percent injected dose per gram of tissue (%ID/g). At least three mice were used for each group and time point.

Hematoxylin & eosin (H&E) and acid-fast (AFB) stains were performed to visualize tissue histology and bacteria, respectively. Von Kossa and Alizarin Red stains were used to detect microcalcification in lung tissues [16, 17].

Statistical comparisons were performed using a two-tailed Student's *t* test (GraphPad Software, Inc.).

Results

Pulmonary implantation 1 day post-infection was 1.94±0.33 $\log_{10}$ CFU. Mice were evaluated at 8 (acute) and 28–36 weeks (chronic) post-infection with corresponding pulmonary bacterial burdens of 7.38±0.94 and 6.51±2.72 $\log_{10}$ CFU.

Na[^{18}F]F PET/CT imaging of *M. tuberculosis*-infected (acute and chronic) and uninfected mice are shown in Fig. 1. While radio-densities demonstrating TB lesions were clearly visible in the lungs of infected mice (Fig. 1a, b), Na[^{18}F]F PET signal was only noted in the chronically infected mice and co-localized well with the TB lesions visualized on CT (Fig. 1a). As expected, there was a high Na[^{18}F]F uptake in bone. Three-dimensional Na[^{18}F]F PET/CT images of chronically infected, acutely infected, and uninfected mice are shown in supplementary movies 1–3 respectively.

Dynamic Na[^{18}F]F PET imaging suggested a state of equilibrium from 40 to 60 min (Fig. 2) with significantly higher PET signal intensities in the pulmonary lesions of chronically infected mice compared with acutely infected or uninfected animals (Fig. 2a; $P<0.01$). However, there was no difference amongst chronically infected, acutely infected, and uninfected mice in the blood (Fig. 2b; $P>0.21$) or bone (Fig. 2c; $P>0.08$) compartments. *Ex vivo* biodistribution studies confirmed the imaging results (Fig. 3).

We next investigated the presence of calcium in postmortem pulmonary tissues of chronic and acutely infected mice as well as uninfected controls (Fig. 4). As expected, well-defined necrotic granulomatous lesions were noted on H&E staining in the *M. tuberculosis*-infected (acute and chronic) tissues (Fig. 4a). Von Kossa staining for calcium phosphate demonstrated black deposits only in the chronically infected TB lesions (Fig. 4b, c). Alizarin Red forms a complex with calcium resulting in birefringent deposits (red), which were also only visualized in the chronically infected tissues (Fig. 4d). AFB staining demonstrated large numbers of *M. tuberculosis* bacilli in both the acutely and chronically infected tissues (Fig. 4e). Figure 5 shows the chronic TB lesion and the corresponding calcium stains in greater detail.

Discussion

Na[^{18}F]F was introduced in 1962 by Blau *et al*. [18]. After chemisorption onto hydroxyapatite, F-18 is exchanged rapidly for the hydroxyl groups on the surface of the hydroxyapatite matrix [$Ca_{10}(PO_4)_6OH_2$] to form fluoroapatite [$Ca_{10}(PO_4)_6F_2$] [19]. Due to its high affinity for bone, low plasma protein binding, and rapid blood and renal clearance, Na[^{18}F]F PET has excellent diagnostic accuracy for the detection of bone metastases [20].

More recently, Na[^{18}F]F PET imaging has also been used to detect microcalcifications in atherosclerotic plaques [21] and breast cancer tissues [22].

Calcification is a hallmark of chronic TB lesions, and it is often visualized radiologically years to decades after infection [7]. Intracellular calcium in macrophages can rise due to *M. tuberculosis* infection [23], and discrete deposition of calcium salts, predominantly tricalcium phosphate, has been identified in chronic TB lesions [24]. We demonstrate that Na[^{18}F]F PET imaging can be utilized to visualize chronic TB lesions with microcalcifications and differentiate them from acute TB lesions (without calcification). Of note, no calcium deposits were apparent on the CT images. However, Na[^{18}F]F PET is more sensitive than CT for the detection of microcalcifications, and positive Na[^{18}F]F PET without microcalcifications evidenced on CT has been previously reported in breast cancer and coronary artery calcification models [22, 25]. The Na[^{18}F]F PET data was confirmed by the *ex vivo* biodistribution studies. Von Kossa staining for calcium phosphate was utilized initially and demonstrated black deposits only in the TB lesions from chronically infected mice. However, since von Kossa staining alone is not sufficient to determine that mineralization represents calcification [16], we also performed Alizarin Red staining which confirmed these findings. Collectively, these data suggest that chronically infected pulmonary TB lesions in C3HeB/FeJ mice develop microcalcification, and can be visualized and differentiated from acute TB lesions using Na[^{18}F]F PET imaging.

While Na[^{18}F]F PET has not yet been tested in humans to detect or monitor TB lesions, it could provide novel insights into TB pathology, which in humans (and recapitulated by the mouse model used in the current study) is manifest by a wide range of (acute and chronic) lesions that respond differently to TB drugs and other interventions.

Conclusion

Na[^{18}F]F PET can be used as a noninvasive biomarker for the detection of chronic TB lesions. While microcalcifications have been reported previously in chronic TB lesions in large animals [26], they have never been reported in a murine model. C3HeB/FeJ mice represent a pathologically relevant mouse model of TB that develops a spectrum of TB lesions, including chronic lesions with microcalcification, similar to human disease.

Supplementary Material

Refer to Web version on PubMed Central for supplementary material.

Acknowledgments

This study was funded by the National Institutes of Health (NIH) Director's Transformative Research Award R01-EB020539 (S.K.J.) and the NIH Director's New Innovator Award DP2-OD006492 (S.K.J.) as well as R01-HL116316 (S.K.J.). The funders had no role in study design, data collection and analysis, decision to publish, or preparation of the manuscript.

References

1. WHO Global tuberculosis report. [Accessed 21 November] 2014. http://www.who.int/tb/publications/global_report/gtbr14_executive_summary.pdf?ua=1

2. Robbins, SL.; Kumar, V. Robbins and Cotran pathologic basis of disease. 8th. Saunders/Elsevier; Philadelphia: 2010.
3. Johnson DH, Via LE, Kim P, et al. Nuclear imaging: a powerful novel approach for tuberculosis. Nucl Med Biol. 2014; 41:777–784. [PubMed: 25195017]
4. Sathekge M, Maes A, Kgomo M, et al. Use of ^{18}F-FDG PET to predict response to first-line tuberculostatics in HIV-associated tuberculosis. J Nucl Med. 2011; 52:880–885. [PubMed: 21571788]
5. Bagci U, Foster B, Miller-Jaster K, et al. A computational pipeline for quantification of pulmonary infections in small animal models using serial PET-CT imaging. EJNMMI Res. 2013; 3:55. [PubMed: 23879987]
6. Murawski AM, Gurbani S, Harper JS, et al. Imaging the evolution of reactivation pulmonary tuberculosis in mice using ^{18}F-FDG PET. J Nucl Med. 2014; 55:1726–1729. [PubMed: 25082854]
7. Leung AN. Pulmonary tuberculosis: the essentials. Radiology. 1999; 210:307–322. [PubMed: 10207408]
8. Harper J, Skerry C, Davis SL, et al. Mouse model of necrotic tuberculosis granulomas develops hypoxic lesions. J Infect Dis. 201110.1093/infdis/jir786
9. Pan H, Yan BS, Rojas M, et al. Ipr1 gene mediates innate immunity to tuberculosis. Nature. 2005; 434:767–772. [PubMed: 15815631]
10. Davis SL, Nuermberger EL, Um PK, et al. Noninvasive pulmonary [^{18}F]-2-fluoro-deoxy-D-glucose positron emission tomography correlates with bactericidal activity of tuberculosis drug treatment. Antimicrob Agents Chemother. 2009; 53:4879–4884. [PubMed: 19738022]
11. Ordonez AA, Pokkali S, DeMarco VP, et al. Radioiodo-DPA-713 imaging correlates with bactericidal activity of tuberculosis treatments in mice. Antimicrob Agents Chemother. 2014; 59:642–649. [PubMed: 25403669]
12. Davis SL, Be NA, Lamichhane G, et al. Bacterial thymidine kinase as a non-invasive imaging reporter for Mycobacterium tuberculosis in live animals. PLoS One. 200910.1371/journal.pone.0006297
13. Weinstein EA, Liu L, Ordonez AA, et al. Noninvasive determination of 2-[^{18}F]-fluoroisonicotinic acid hydrazide pharmacokinetics by positron emission tomography in Mycobacterium tuberculosis-infected mice. Antimicrob Agents Chemother. 2012; 56:6284–6290. [PubMed: 23006755]
14. Weinstein EA, Ordonez AA, DeMarco VP, et al. Imaging Enterobacteriaceae infection *in vivo* with ^{18}F-fluorodeoxysorbitol positron emission tomography. Sci Transl Med. 2014:259ra146.
15. Foss CA, Harper JS, Wang H, et al. Noninvasive molecular imaging of tuberculosis-associated inflammation with radioiodinated DPA-713. J Infect Dis. 2013; 208:2067–2074. [PubMed: 23901092]
16. Bonewald LF, Harris SE, Rosser J, et al. von Kossa staining alone is not sufficient to confirm that mineralization *in vitro* represents bone formation. Calcif Tissue Int. 2003; 72:537–547. [PubMed: 12724828]
17. Lievremont M, Potus J, Guillou B. Use of alizarin red S for histochemical staining of Ca2+ in the mouse; some parameters of the chemical reaction *in vitro*. Acta Anat. 1982; 114:268–280. [PubMed: 7158284]
18. Blau M, Nagler W, Bender MA. Fluorine-18: a new isotope for bone scanning. J Nucl Med. 1962; 3:332–334. [PubMed: 13869926]
19. Blau M, Ganatra R, Bender MA. 18F-fluoride for bone imaging. Semin Nucl Med. 1972; 2:31–37. [PubMed: 5059349]
20. Shen CT, Qiu ZL, Han TT, Luo QY. Performance of ^{18}F-fluoride PET or PET/CT for the detection of bone metastases: a meta-analysis. Clin Nucl Med. 2014; 40:103–110. [PubMed: 25290289]
21. Joshi NV, Vesey AT, Williams MC, et al. ^{18}F-fluoride positron emission tomography for identification of ruptured and high-risk coronary atherosclerotic plaques: a prospective clinical trial. Lancet. 2014; 383:705–713. [PubMed: 24224999]
22. Wilson GH 3rd, Gore JC, Yankeelov TE, et al. An approach to breast cancer diagnosis via PET imaging of microcalcifications using ^{18}F-NaF. J Nucl Med. 2014; 55:1138–1143. [PubMed: 24833491]

23. Jayachandran R, Sundaramurthy V, Combaluzier B, et al. Survival of mycobacteria in macrophages is mediated by coronin 1-dependent activation of calcineurin. Cell. 2007; 130:37–50. [PubMed: 17632055]

24. Canetti, G. The histobacteriogenesis of tuberculosis lesions: experimental studies. Springer Publishing Company, Inc; New York: 1955. The tubercle bacillus in the pulmonary lesion of man; p. 87-90.

25. Dweck MR, Chow MW, Joshi NV, et al. Coronary arterial ^{18}F sodium fluoride uptake: a novel marker of plaque biology. J Am Coll Cardiol. 2012; 59:1539–1548. [PubMed: 22516444]

26. Gomori G. Calcification and phosphatase. Am J Pathol. 1943; 19:197. [PubMed: 19970686]

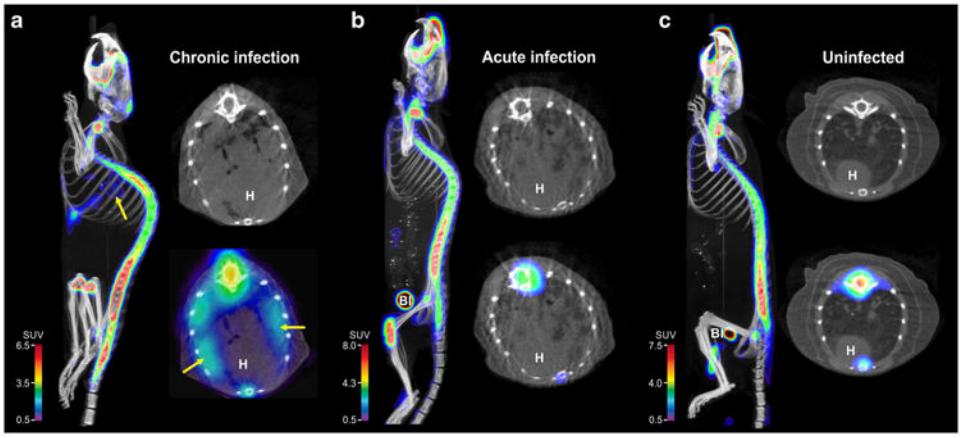

Fig. 1.

Transverse, coronal, and sagittal sections from Na[^{18}F]F PET/CT imaging performed on **a** chronically *M. tuberculosis*-infected, **b** acutely *M. tuberculosis*-infected, and **c** uninfected mice, 40 min post tracer injection. Radio-densities demonstrating TB lesions are clearly visible in the lungs of infected mice (**a** and **b**), but Na[^{18}F]F PET signal is only noted in the chronically infected mice (*arrows*). Na[^{18}F]F PET signal is also noted in bones and the urinary bladder (*Bl*). *H* heart.

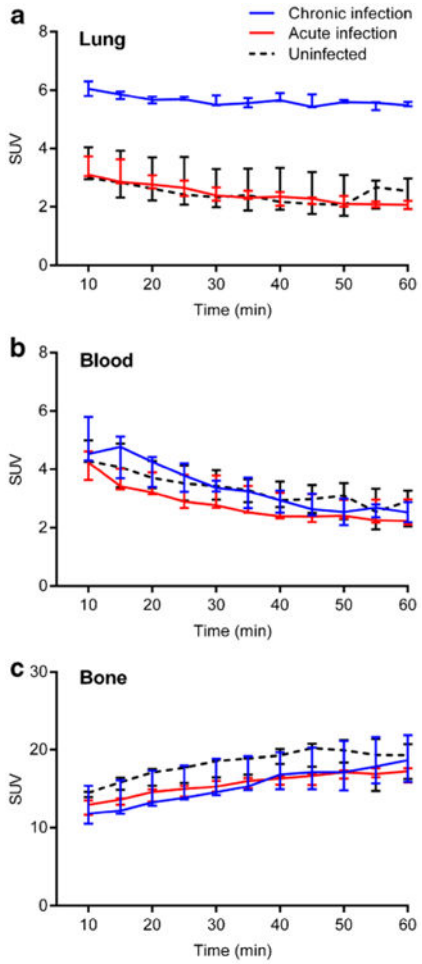

Fig. 2.

Dynamic Na[^{18}F]F PET imaging demonstrates significantly higher signal in a pulmonary lesions from chronically infected mice (*blue*) compared with acutely infected (*red*) or uninfected (*dotted black*) animals. No difference is evident in **b** the blood or **c** bone compartments amongst the three different groups. Three animals were imaged for each group. Data is represented as median and interquartile range.

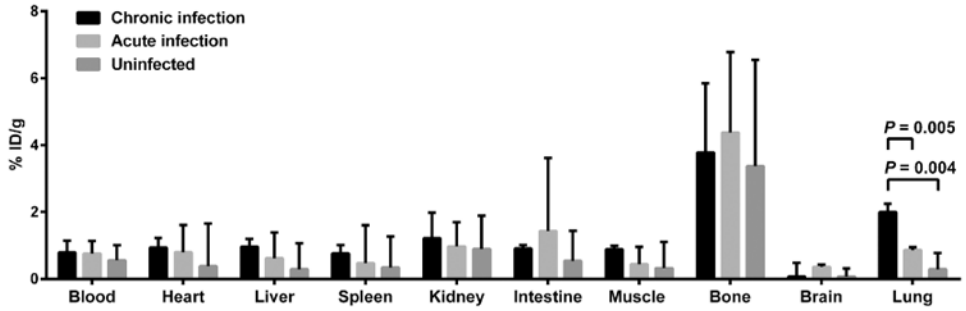

Fig. 3.

Ex vivo biodistribution studies performed after completion of imaging. Na[^{18}F]F uptake is significantly higher in the chronically infected lung tissues, while uptake is similar amongst the three different groups in other tissue compartments. Three animals were used for each group. Data is represented as median and interquartile range.

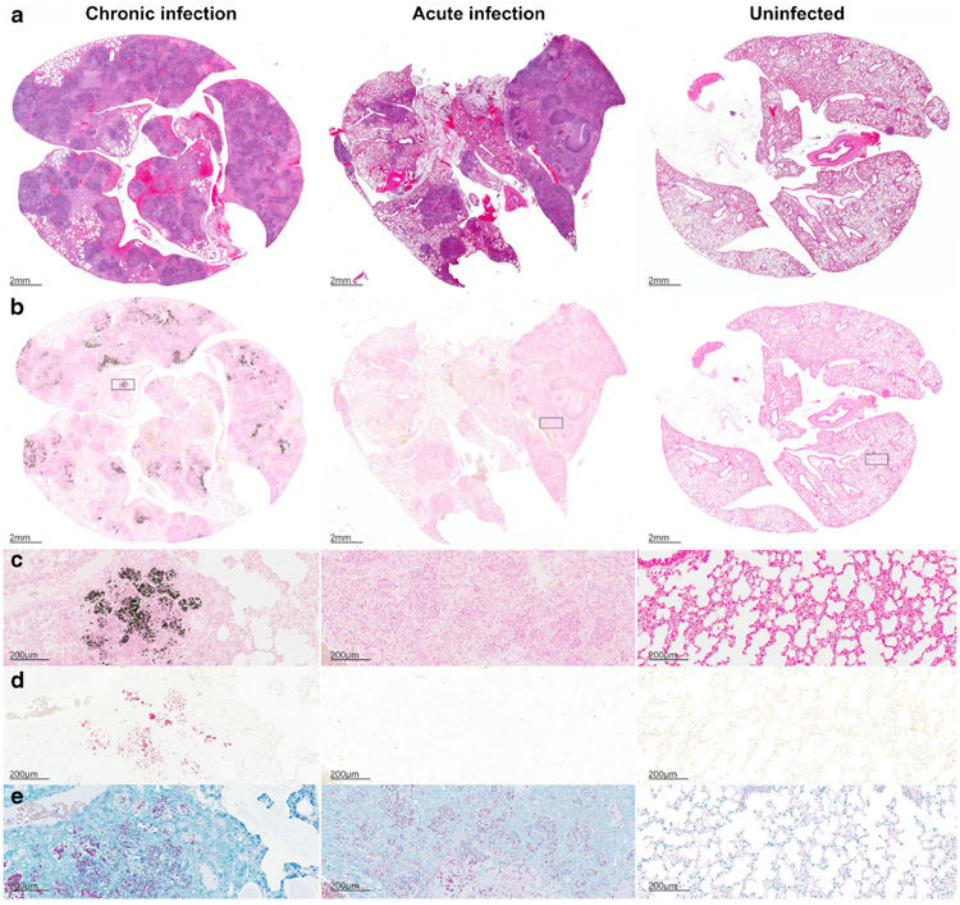

Fig. 4.

Histology sections from chronic (*left panels*) and acutely infected (*middle panels*) mice and uninfected (*right panels*) controls are shown. H&E staining (**a**), von Kossa staining for calcium phosphate deposits in *black* (**b** and **c**), Alizarin Red with calcium deposits visualized in red (**d**), and acid-fast staining for *M. tuberculosis bacilli* (**e**). Well-defined necrotic granulomas are noted on H&E staining in the *M. tuberculosis*-infected (acute and chronic) tissues. Von Kossa and Alizarin Red staining demonstrate deposits only in TB lesions from chronically infected tissues (**b–d**). AFB staining demonstrates large numbers of bacilli in infected (acute and chronic) tissues (**e**).

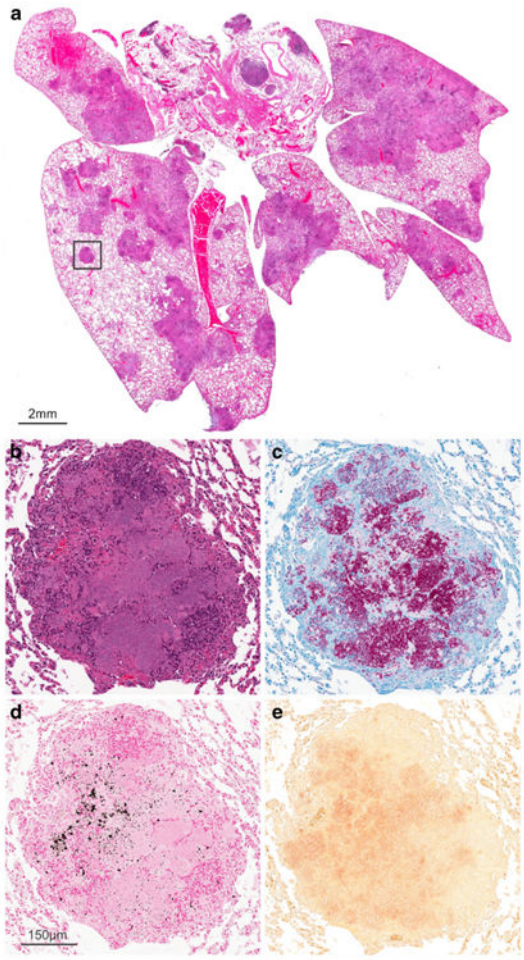

Fig. 5.

a Histology demonstrating pulmonary lesions in a *M. tuberculosis*-infected mouse with chronic infection. Higher magnification of a TB lesion (*inset*) demonstrates a classic granulomatous lesion with central necrosis (**b**) and a large number of *M. tuberculosis* bacilli seen with AFB staining (**c**). Microcalcifications represented as *black* and *red* deposits are evident on von Kossa (**d**) and Alizarin Red staining (**e**), respectively.